Bedrock reconstruction from free surface data for unidirectional glacier flow with basal slip.

Elizabeth K. McGeorge · Mathieu Sellier · Miguel Moyers-Gonzalez · Phillip L. Wilson

Abstract Glacier ice flow is shaped and defined by several properties, including the bedrock elevation profile and the basal slip distribution. The effect of these two basal properties can present in similar ways in the surface. For bedrock recovery this makes distinguishing between them an interesting and complex problem. The results of this paper show that in some synthetic test cases it is indeed possible to distinguish and recover both bedrock elevation and basal slip given free surface elevation and free surface velocity. The unidirectional shallow ice approximation is used to compute steady state surface data for a number of synthetic cases with different bedrock profiles and basal slip distributions. A simple inversion method based on Newton's method is applied to the known surface data to return the bedrock profile and basal slip distribution. In each synthetic test case, the inversion was successful in recovering both the bedrock elevation profile and the basal slip distribution variables. These

E. K. McGeorge
School of Mathematics and Statistics
University of Canterbury
Christchurch, New Zealand
ORCID: 0000-0001-5707-640X

M. Sellier
Department of Mechanical Engineering
University of Canterbury
Christchurch, New Zealand
ORCID: 0000-0002-5060-1707

M. Moyers-Gonzalez (✉)
School of Mathematics and Statistics
University of Canterbury
Christchurch, New Zealand
Tel.: +64-64-3-364-2987
E-mail: miguel.moyersgonzalez@canterbury.ac.nz
ORCID: 0000-0003-4817-1506

P. L. Wilson
School of Mathematics and Statistics
University of Canterbury
Christchurch, New Zealand
ORCID: 0000-0002-4563-9399

results imply that there is a unique bedrock profile and basal slip which give rise to a unique combination of free surface velocity and free surface elevation.

Keywords Glacier · Ice flows · Inverse problems · Shallow Ice Approximation · Basal slip

1 Introduction

Understanding cryosphere dynamics is key to modelling climate change. The contribution of land ice to global mean sea level (GLMS) rise for medium emissions scenarios is projected to be at least 0.10 m with some models predicting a contribution of up to 0.27 m [10]. Cazenave et al. (2013) identified one of the main contributors to this rise as the melting of glaciers. Glaciers are also important socially, with millions of people in the Himalaya, Karakoram and Hindu Kush mountains relying on glacial reserves for their drinking water [36]. Given the potentially large impact of glacier dynamics on human livelihood, comprehensive glacier models are needed. In particular, accurate methods for calculating the total ice mass of glaciers are required. If the bedrock profile of the glacier is known, the resulting ice thickness can be used to calculate the mass of the ice for that particular glacier. Having explicit knowledge of glacier mass can be useful and influential in policy and natural resource planning. However, due to the difficulty of measuring the bedrock profile explicitly in many cases, it is desirable to use surface measurements and an inversion model to predict the bedrock elevation.

Surface elevation and free surface velocity data are already recorded for many ice flows and glaciers. A number of parties collect and collate data such as the World Glacier Inventory (WGI), the United States Snow and Ice Data Center (NSIDC) and the Global Land Ice Measurements from Space (GLIMS) initiative. Data is collected in a variety of ways, primarily in-situ or via air- or space- borne craft [15]. Due to the large availability of surface data, bedrock recovery methods using these free surface measurements are particularly popular. Another feature that can be measured or calculated from surface data is the accumulation/ablation distribution for the glacier. This distribution describes how the glacier grows/diminishes over time dues to snow/ice accumulation/ablation over time. This paper assumes this distribution to be measurable, though it may difficult and time consuming to do so. Field measurements can be costly [27, 23]. Accurately predicting the accumulation rate from other measurable surface variables is an area of research in and of itself and many different methods employing a vast array of techniques have been proposed [e.g. 13, 29, 4, 37].

Glaciers exhibit gravity-driven creep flow which is sustained by the underlying sloped geography. Glacier ice is categorised as an incompressible, nonlinear, viscous, heat conducting fluid [21] which can be described mathematically by the full Stokes flow equations together with rheological laws. Many methods of approximating the Stokes flow equations have been proposed in the last century. One of the most widely used approximations is the shallow-ice approximation (SIA) [24, 18]. In the SIA model, gravity-driven ice flow is solely balanced by basal drag neglecting longitudinal and transverse stresses, as well as vertical stress gradients [1]. Due to the complex nature of glacier ice flow, recovering the glacier ice thickness from only surface measurements is a non-trivial inverse problem. Variations in recovered glacier ice thickness can be as large as the ice thickness recovered for different models. The recovered thickness is also very sensitive to input data [16]. In addition, inversion methods can have ill-defined solutions and may impose too many assumptions, such as the no-slip condition at the base [5, 40, 2, 19, 22].

Imposition of a no-slip condition simplifies the inverse problem significantly and allows much faster computation. However, basal slip is known to be influential in the flow

behaviour [26] and so is important to include if possible. Since the primary driving force of glacier flow is gravity, flow speed is modulated by presence, or lack thereof, of friction at the glacier-bedrock boundary [14]. In a temperate glacier, where high temperatures cause melt, or a thick glacier, where increased regelation causes melt, the glacier-bedrock interface is wet which can cause the ice to slide along the interface easily. Conversely in a glacier which has a frozen base, the ice flow is stuck to the ground and does not slide [7]. Other factors such as till composition also impact the amount of friction at the base. Increased velocity at the base results in a lower steady state glacier surface due to a process called dynamic thinning; the loss of ice due to accelerated ice flow into the ablation zone [6, 17, 35, 38]. Dynamic thinning can also be caused by a steeper bedrock profile simply due to the increased contribution of gravity on the glacial flow.

Since the free surface of an ice flow is affected by both basal slip and bedrock topography, separating the effects of these two factors in the recovery is difficult [32, 33]. This paper seeks to accurately recover the bedrock topography of a synthetic glacier with non-constant basal slip given known free surface elevation and velocity. The method proposed builds on the work of [19] by modifying their method to include basal slip.

An overview of the governing ice flow model used is given in Sect. 2. Section 3 constructs the synthetic glacier surface for a number of different synthetic cases. The results affirm that both basal slip distribution and bedrock profile have a significant effect on the resultant steady state surface elevation and free surface velocity. Section 4 gives the derivation of the recovery method proposed and the results of implementing this are given in Sect. 5. A brief sensitivity analysis of the method to noisy surface data is given in Sect. 6. Finally, the results are discussed in Sect. 7 and final conclusions are drawn in Sect. 8.

2 Governing model

This paper assumes the glacier flow dynamics are well described by the SIA. The SIA simplifies the full Stokes equations by performing a scaling analysis to obtain dimensionless field equations for the glacier flow. The small parameter used assumes the glacier extent is much larger than its thickness. Some properties of the SIA model are; (1) longitudinal and transverse stresses, as well as vertical stress gradients vanish,(2) the horizontal component of the velocity points in the direction of steepest descent of the free surface and does not change with depth, and (3) domes or troughs have no horizontal velocity. Blatter et al. [8] advise caution when applying the SIA to processes on smaller scales where the assumptions may no longer be valid, for example, anisotropic basal sliding or locally steep basal topography. Despite potential drawbacks, the SIA is used widely in ice flow modelling as it reduces a three dimensional flow problem into a two dimensional problem. This makes computationally simple in comparison to higher order models such as (ADD: more higher order models) the full Stokes where a full force balance has to be calculated at each step. The SIA is typically set up with x-direction along the flow, the y-direction as the transverse direction, and the z-direction as the upward direction normal to the gravitational field. To simplify the testing of the new inversion method, the SIA is restricted to the unidirectional case which omits the transverse flow.

Table 1: Notation.

Symbol	Meaning
z	Vertical axis, represents height above a reference elevation
x	Horizontal axis, distance along glacier from an upstream reference
t	Time
H	Glacier height
S	Glacier surface
z_b	Bedrock profile elevation
a	Accumulation ablation profile for the glacier
u	Velocity profile of the glacier
u_b	Basal velocity
u_s	Free surface velocity
τ	Stress
τ_b	Basal shear stress
β	Basal slip distribution

2.1 Derivation of equations

The glacier height, H, is related to the surface S and the bedrock elevation z_b via

$$H = S - z_b \tag{1}$$

at any time, t. See Fig. 1 for a pictorial description of this relationship.

By considering the momentum balance, volume flux, and mass conservation of the glacier, the expression for height evolution in the unidirectional case is

$$\frac{\partial H}{\partial t} = a(x) - \frac{\partial}{\partial x} q_x, \tag{2}$$

where $a(x)$ is the accumulation/ablation function of the glacier in meters of water equivalent per year, and

$$q_x = \int_{z_b}^{S} u_x dz \tag{3}$$

describes the ice flux by integrating the velocity of the ice along the x-direction, u_x, from the bedrock to the free surface. Following Gessese et al. [19] and adapting to include basal slip velocity u_b, the velocity profile is given by

$$u_x(z) = \frac{1}{2} A(\rho g)^3 \left(\frac{\partial S}{\partial x} \right)^3 \left[(S-z)^4 - H^4 \right] + u_b(x), \tag{4}$$

where ρ is the ice density, g is the acceleration due to gravity and A is the creep or flow parameter given in Table 2. Values for these constants are given in Table 2. The value for ρ is taken as the midpoint of the range for glacier ice as recommended by Cuffey and Patterson [14, Table 2.1].

The no-slip condition classically imposed [5, 40, 2, 19, 22] forces $u_b = 0$ for the glacier. This reduces the amount of surface data required for the inverse problem as without slip the
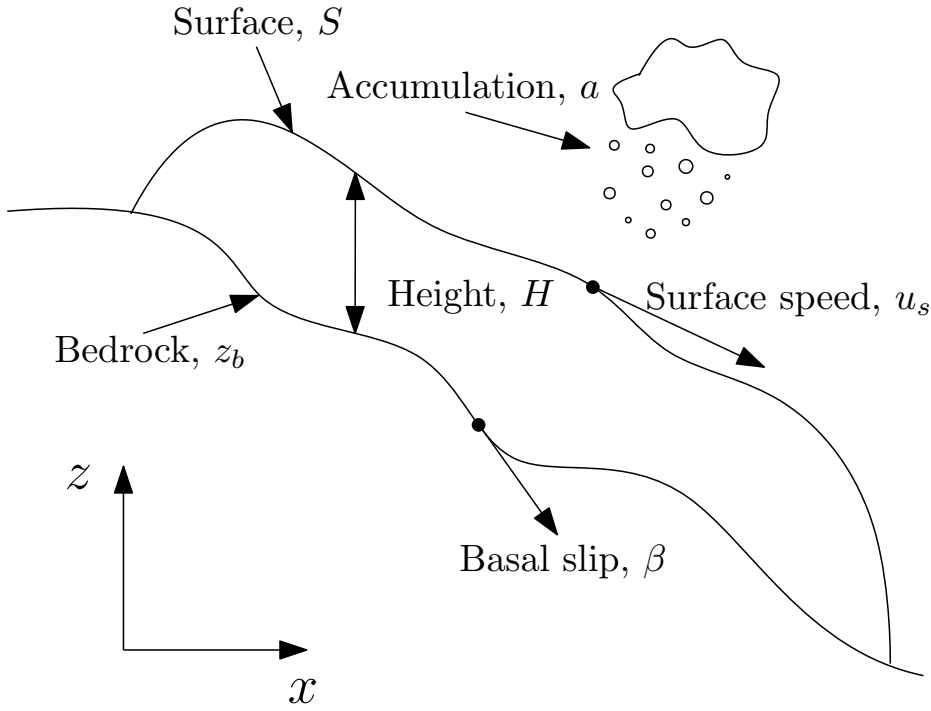
Fig. 1: Glacier flowing downstream with surface S and bedrock z_b and thickness or height H. Surface speed, u_s is indicated at the glacier surface and basal slip, β is indicated at the glacier base. Accumulation, a, is represented as falling snow.

system has only one unknown to recover. However, as discussed in the introduction, basal slip can have significant effect on glacier height which reduces the practical applications if it is neglected. Here, no such condition is imposed and the glacier is allowed to have varied basal slip along the base of the glacier.

Weertman [39] first proposed a power-type law for basal shear on a hard bed and both Fowler [18] and Lliboutry [31] proposed a more general form of the law for a flow with cavity formation. Budd et al. [9] found this generalised form to be empirically true for ice flow with basal shear described by

$$\tau_b^3 = \frac{1}{A_s} u_b,$$

(5)

where τ_b is the shear stress, A_s the sliding constant given in Table 2, and u_b the basal velocity. The value for A_s is taken from Gessese et al. [19].

Considering also Glen's empirical law for the shear rate [20] and Nye's adaption of the law to ice flow [34], at the ice flow base gives

$$\left. \frac{\partial u}{\partial z} \right|_{z=z_b} = A\tau_b^3.$$

(6)

The value assigned to A depends strongly on temperature. The value given in Table 2 is for an ice sheet at $-5 \deg C$ and was recommended by Cuffey and Patterson [14, Table 3.4]. The

Table 2: Typical values of constants used throughout.

Symbol	Name	Value
A_s	Sliding coefficient	5×10^{-14} m^8 N^{-3} yr^{-1}
A	Glen's law parameter	4.16×10^{-17} Pa^{-3} yr^{-1}
ρ	Ice density	880 kg m^{-3}
g	Gravitational acceleration	9.81 m s^{-2}

derivation of the SIA gives

$$\tau_b = -\rho g H \frac{\partial S}{\partial x}, \tag{7}$$

which combines with (5)and (6) to give the following expression for basal velocity

$$u_b(x) = -\beta(x) A_s (\rho g)^3 H(x)^3 \left(\frac{\partial S(x)}{\partial x} \right)^3, \tag{8}$$

where $\beta(x)$ is the basal slip distribution which regulates the amount of basal slip at the glacier base. Basal slip is restricted such that $\beta(x) \in [0, 1]$ for all x in the glacier domain. Physically, $\beta(x) = 0$ represents a sticky base and $\beta(x) = 1$ a friction-less base. It is not required for $\beta(x)$ to be constant along the glacier length.

Combining (4) and (8) gives a full expression for the velocity profile. This velocity profile is substituted into (3) to give the ice flux. Finally, substituting this ice flux into the mass balance gives a non-linear diffusion equation

$$\frac{\partial H}{\partial t} = a + \frac{2}{5} (\rho g)^3 \frac{\partial}{\partial x} \left(D \frac{\partial S}{\partial x} \right) \tag{9}$$

with non-linear effective diffusion coefficient D given by

$$D = \left| \frac{\partial S}{\partial x} \right|^2 H^4 \left[AH + \frac{5}{2} \beta A_s \right]. \tag{10}$$

Note that the full velocity profile easily gives an expression for the surface velocity by setting $z = S$:

$$u_s = -(\rho g)^3 \left(\frac{\partial S}{\partial x} \right)^3 H^3 \left(\frac{1}{2} AH + \beta A_s \right). \tag{11}$$

3 Direct problem methodology

Investigating the inverse problem requires synthetic surface data for basic ice flows. This data is produced by solving (9) for the steady state using a slight modification of the finite difference scheme as laid out by Gessese et al. [19]. The scheme discretizes Eq. (9) in time using an Euler explicit scheme and spatially using a second-order accurate central finite difference scheme. The results is

$$\begin{aligned} H_i^{n+1} = H_i^n + \Delta t a_i + \frac{\Delta t}{2 \Delta x} \frac{2}{5} (\rho g)^3 &\left\{ (D_{i+1}^n + D_i^n) \right. \\ &\left. \left(\frac{S_{i+1}^n - S_i^n}{\Delta x} \right) - (D_i^n + D_{i-1}^n) \left(\frac{S_i^n - S_{i-1}^n}{\Delta x} \right) \right\}, \end{aligned} \tag{12}$$

where

$$D_i = H_i^4 \left| \frac{S_{i+1} - S_{i-1}}{2\Delta x} \right|^2 \left(AH_i + \frac{5}{2}\beta A_s \right).$$ (13)

The scheme is implemented in forwards time with a mesh size of $\Delta x = 1$ m and $\Delta t = 0.00004$ yrs. At each time step the surface is calculated via $S_i = (z_b)_i + H_i$. The scheme runs until a steady state is achieved as defined by

$$\max_i |H_i^{n+1} - H_i^n| < 0.001 \text{ m}.$$ (14)

This steady state represents an equilibrium between the accumulation and ablation due to a steady flow of ice. Note that the scheme was tested for stability with three other grid resolutions to confirm stability; $\Delta x = 50$ m, $\Delta t = 0.1$ yrs, $\Delta x = 20$ m, $\Delta t = 0.016$ yrs, and $\Delta x = 5$ m, $\Delta t = 0.001$ yrs. This steady state surface is computed for a number of benchmark cases as outlined in Subsect. 3.2.

In each case the glacier starts with no height, $H(x,0) = 0$, and has Dirichlet boundary conditions, $H(0,t) = H(L,t) = 0$. These conditions represent that there is no height at both the top and bottom of the glacier.

3.1 Benchmark cases

Combinations of different accumulation/ablation rate, basal slip distribution, and bedrock elevation profile are used as benchmark cases for testing the methods.

3.1.1 Choice of accumulation/ablation rate, $a(x)$

For each benchmark case the accumulation/ablation function is defined as

$$a(x) = \begin{cases} a_0 \left(1 - \frac{300-x}{100} \right) & \text{if} \quad x \le 300 \\ a_0 \left(\frac{2200-x}{1900} \right) & \text{if} \quad x \ge 300 \end{cases}$$ (15)

where a_0 is the maximum value of the accumulation/ablation function and set to 0.5 for all future calculations. Adjusting this maximum values simply raises or lowers the steady state surface [30]. This function gives the most accumulation at the top end of the glacier and then linearly decreases along it's length until at the bottom end which has net ablation.

3.1.2 Cases of basal slip distribution, $\beta(x)$

Three different types of basal slip distributions are tested. The different distributions again help to test the robustness of the method against more realistic scenarios. The three type are labelled and mathematically defined as follows. Examples of their shapes are given in Fig. 2.

1. $\beta(x)$ constant.
   This type of slipping gives constant slip along the glacier as described by

   $$\beta(x) = K,$$ (16)

   where K is a constant in $[0,1]$. $K = 0$, for example, could represent a cold-based glacier in which the ice is frozen to the bed which inhibits the flow mechanisms of sediment deformation, ice deformation and basal sliding [28, 3, 25, 11].

2. $\beta(x)$ bump.

This type of slip gives negligible slip at the top and bottom of the glacier with narrow region with lots of slip in the middle as described by

$$\beta(x) = \gamma e^{\frac{-(x-M)^2}{\delta^2}}, \tag{17}$$

where M is the midpoint of the bump, γ is the height of the bump and δ is the extent.

3. $\beta(x)$ step.

This type of slipping gives a transition from negligible basal slip to some slip as described by

$$\beta(x) = \frac{R}{1 + e^{k(x-M)}}, \tag{18}$$

where $\lim_{x \to \infty} \beta(x) = R$ and $\lim_{x \to -\infty} \beta(x) = 0$, k is the steepness and M is the midpoint of the transition between asymptotes.
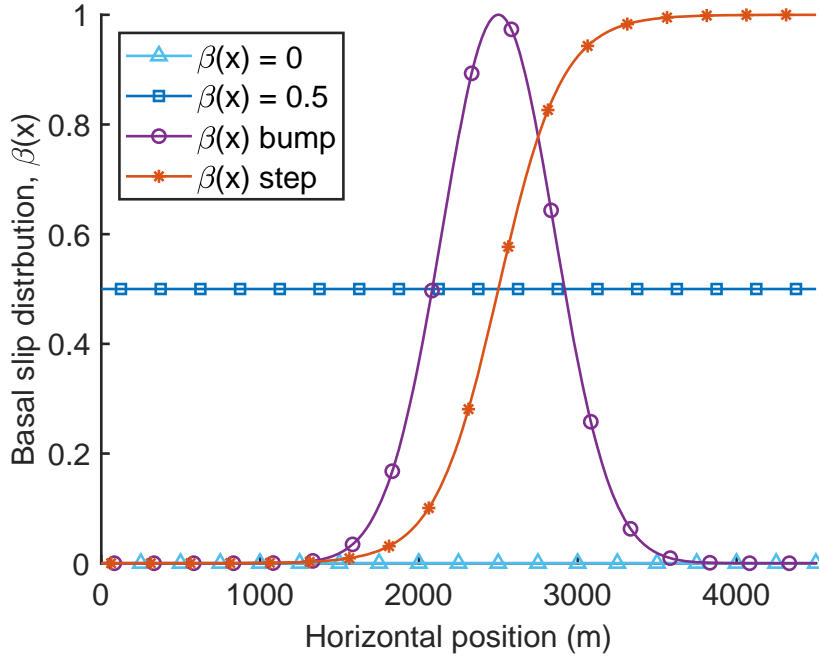
Fig. 2: Examples of the three forms of basal slip distribution, $\beta(x)$. For $\beta(x)$ bump, $\gamma = 1, M = 2500, \delta = 500$. For $\beta(x)$ step, $L = 0, R = 1, M = 2500, k = 0.005$.

3.1.3 Cases of bedrock elevation profile, $z_b(x)$

Two different bedrock elevation profiles are defined in the benchmark cases. The two forms are given by:

1. An inclined flat bed, $z_b = f$

$$z_b(x) = f(x) = z_0 - \alpha x \qquad (19)$$

where z_0 is the elevation at the point $x = 0$ and α is the slope.

2. An inclined bumpy bed, $z_b = b$

$$z_b(x) = b(x) = z_0 - \alpha x + A\sin(\lambda x); \qquad (20)$$

where z_0 and α are as before, A is the amplitude of the bumps and λ wavelength. For all simulations, $A = 50$ and $\lambda = \frac{1}{350}$. This bedrock profile is designed to combine two test cases as used by Gessese et al. [19] to test their no-slip recovery method.

In each case $z_0 = 900$ m and $\alpha = 0.2$.

3.2 Resultant steady state surfaces for each type of basal slip.

Figures 3 to 6 give the resultant steady state surfaces for each type of basal slip for the two cases of bedrock profile. In each plot, the underlying basal slip is indicated by the marker type which matches those used in Fig. 2.

In Figs. 3 and 4, the case of no-slip, $\beta(x) = 0$, is plotted along side the constant slip case and is consistent with the results of Gessese et al. [19]. These two figures illustrate that increased basal slip results in: (1) a glacier with less height and, (2) an elongated glacier domain. These two effects are consistent with literature [35, 6] and occur for the other types of basal slip also but are less visibly obvious. Figure 4 shows that the glacier surface profile follows that of the bedrock.

In Fig. 5, a visible dip occurs in the glacier surface at the location of increased basal slip for the bump case. Similarly, the glacier surface is observed to lower once the transition occurs to more basal slip in the step case. In Fig. 6 the same properties are exhibited due to changes in basal slip but are much harder to see due to the surface undulations produced by the bedrock.

These modelled surfaces show that the shape of the glacier is affected by both the bedrock and the basal slip. Without accounting for basal slip, the dips observed in the surface will appear to be the result of related dips in the bedrock. These results for the direct case reinforce the importance of including basal slip in the recovery method for bedrock elevation.

4 Inverse methodology

The inverse problem seeks to recover the bedrock elevation profile, $z_b(x)$ and the basal slip distribution, $\beta(x)$, for a steady state glacier from two known free surface quantities; (1) the surface elevation, S, and (2) the free surface velocity, u_s. Previous authors [19, 22] have recovered bedrock data from one free surface input with the assumption of a sticky, no-slip base where $\beta(x) = 0$. Using two input variables allows for the recovery of bedrock elevation profile and basal slip distribution simultaneously. As with the direct problem, the flow is assumed well described by the unidirectional SIA defined in Eq. (9) and the surface velocity approximated by Eq. (11).

Glaciers and ice flows have been studied extensively throughout the past century by a variety of different groups such as NSIDC. Data collection has been pushed particularly due
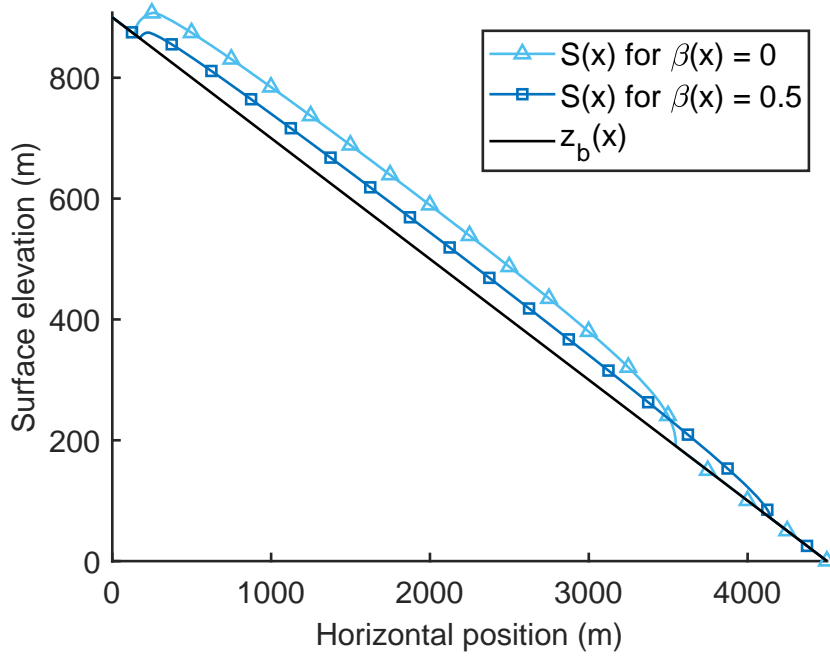
Fig. 3: Computed steady state glacier surfaces for constant basal slip with flat inclined bedrock, $z_b = f$.

to ice melt acting as a major contributor to sea level rise [12] (Fig. 13.10, 13.13). As such the body of data for glaciers and ice flows is ever increasing. It is reasonable to assume there is, or can be measured, sufficient data for the two free surface variables as well as the accumulation ablation function.

4.1 Method for the inverse problem

Given two observable variables, u_s and S, the following will show that it is possible to accurately recover to unknown variables, $H(x)$ and $\beta(x)$. Recovery of $H(x)$ immediately gives the desired bedrock due to Eq. (1). To solve for these two variables, first consider the equations which define them. The steady state surface is given by Eq. (9) where $\partial H / \partial t$ is set to 0,

$$0 = a + \frac{2}{5}(\rho g)^3 \frac{\partial}{\partial x} \left(\left| \frac{\partial S}{\partial x} \right|^2 H^4 \left[AH + \frac{5}{2} \beta A_s \right] \frac{\partial S}{\partial x} \right) \tag{21}$$
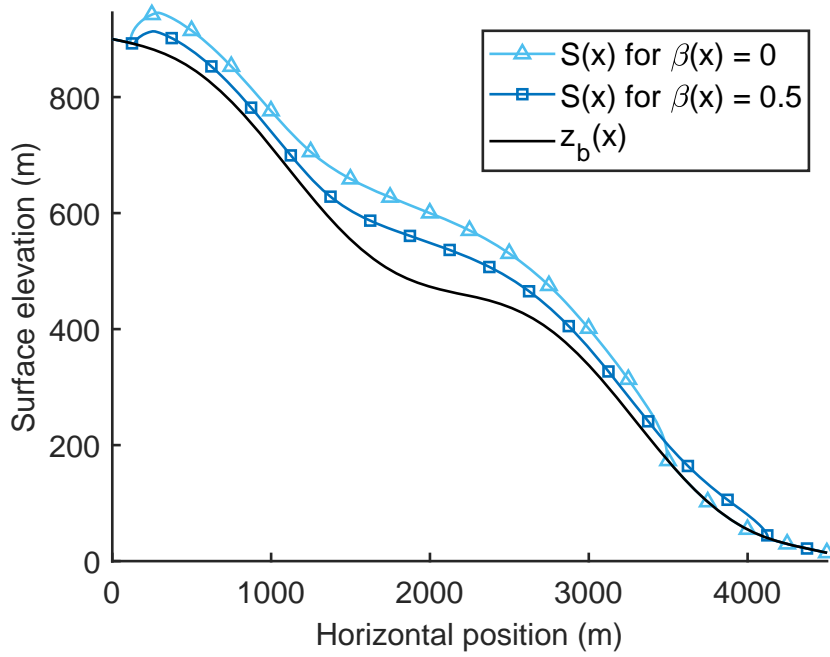
Fig. 4: Steady state glacier surfaces for constant basal slip with bumpy inclined bedrock, $z_b = b$.

which has two unknowns H and β. Since the free surface velocity is also given, rearranging the equation for β gives

$$\beta = \frac{-1}{A_s} \left(\frac{u_s}{(\rho g)^3 \left| \frac{\partial S}{\partial x} \right|^2 \frac{\partial S}{\partial x} H^3} + \frac{1}{2} AH \right) \tag{22}$$

Substituting this expression for β into the steady state surface equation above and integrating results in

$$0 = \int_0^x a \, dx - \frac{1}{10} (\rho g)^3 \left| \frac{\partial S}{\partial x} \right|^2 \frac{\partial S}{\partial x} AH^5 - u_s H + C_0 \tag{23}$$

which is a polynomial equation in only H with constant of integration

$$C_0 = - \int_0^{x_0} a \, dx + \frac{1}{10} (\rho g)^3 \left[\left| \frac{\partial S}{\partial x} \right|^2 \frac{\partial S}{\partial x} \right] \Bigg|_{x=x_0} AH_0^5 + (u_s)_0 H_0 \tag{24}$$

where x_0 is some point inside the domain of the glacier where the height is known. It is reasonable to assume height can be known at one location from practical measurements.

There are numerous methods which could be employed to solve the polynomial for H. Newton's method is chosen for it's simplicity and controllability. Hence solving (23) for
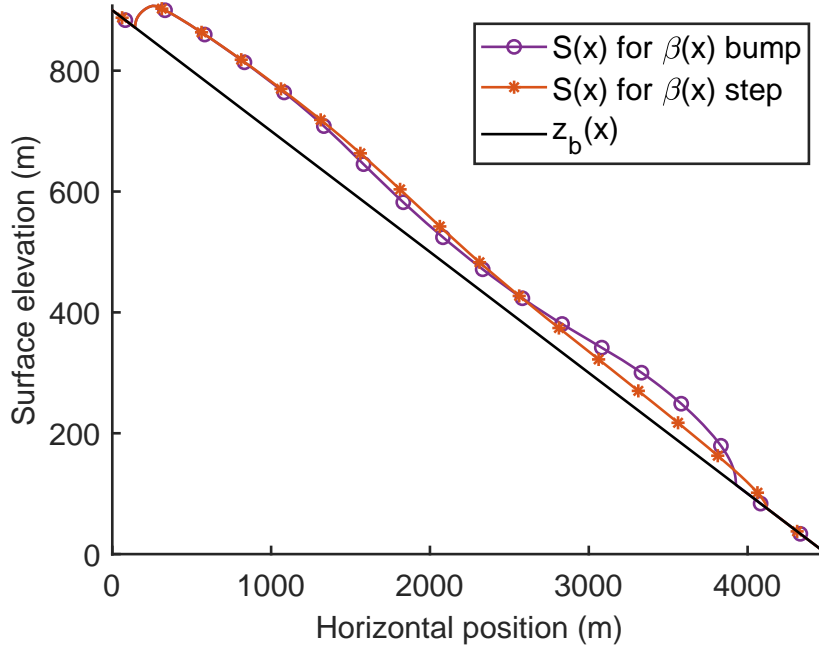
Fig. 5: Steady state glacier surfaces for basal slip with a bump and basal slip with a step where $z_b = f$.

each $H_i = H(x_i)$ using Newton's method

$$H_i^{n+1} = H_i^n - \frac{F(H_i^n)}{F'(H_i^n)} \tag{25}$$

with the following functions

$$F(H_i) = \int_0^{x_i} a\,dx - \frac{1}{10}(\rho g)^3 \left(\frac{\partial S}{\partial x}\right)^3 \Bigg|_{x=x_i} AH_i^5 - (u_s)_i H_i + C_0 \tag{26}$$

$$F'(H_i) = -\frac{5}{10}(\rho g)^3 \left(\frac{\partial S}{\partial x}\right)^3 \Bigg|_{x=x_i} AH_i^4 - (u_s)_i. \tag{27}$$

For Newton's method to find the correct root of F it is important to start with a nearby guess. Therefore, the method will move away from x_0 to the left and right using

$$H_i = H_0 \qquad\qquad \text{for } x_i = x_0 \tag{28}$$

$$H_i^0 = H_{i-1} \qquad\qquad \text{for } x_i > x_0 \tag{29}$$

$$H_i^0 = H_{i+1} \qquad\qquad \text{for } x_i < x_0 \tag{30}$$

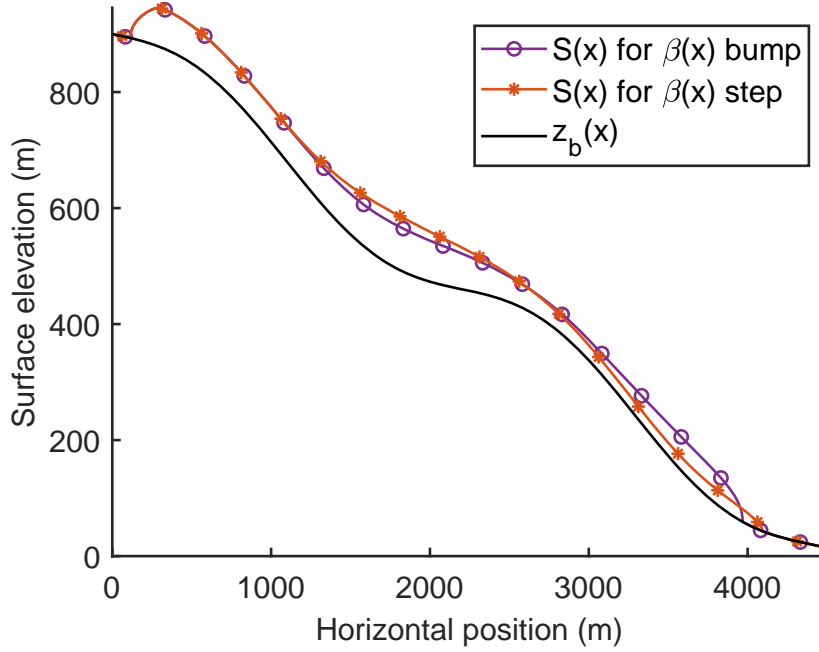For each glacier, x_0 is chosen to be in the middle of the glacier domain.

Fig. 6: Steady state glacier surfaces for basal slip with a bump and basal slip with a step where $z_b = b$.

5 Results

Figures 7 to 10 show the inversion results for each combination of underlying bedrock and basal slip distribution. The recovered bedrock profile elevation, $z_{b,rec}$, is shown in each sub-fig. (a). The recovered basal slip distribution, β_{rec}, is shown in in each subfig. (b). The recovered variables in each case are overlaid on the true variables for easy comparison.

Table 3 gives relative errors for the recovered bedrock and basal slip distribution respectively. The relative error between the recovered variables, x_{rec}, and the true value, x, is calculated by

$$E(x_{rec}, x) = \frac{||x_{rec} - x||_2}{||x||_2} = \frac{\sqrt{\sum_i ((x_{rec})_i - x_i)^2}}{\sqrt{\sum_i x_i^2}}, \tag{31}$$

where i runs along the glacier domain. Note that (31) is not defined for $x = 0$. In this case, the error is defined as

$$E(x_{rec}, x) = ||x_{rec}||_2 = \sqrt{\sum_i ((x_{rec})_i)^2}. \tag{32}$$

For each benchmark case, the bedrock reconstruction is in very good agreement with the true profile. The relative errors in bedrock recovery, as given in table 3, are of magnitude

10^{-3} for each case. This indicates that the has high accuracy for recovering bedrock elevation profiles. This is illustrated in each sub-fig. (a) which show close alignment between the recovered bedrock and the true bedrock.

For each benchmark case, the recovered basal slip distribution is in agreement with its true distribution. The relative errors, as given in table 3 are of magnitude 10^{-1} or smaller for each case. While this is a much larger error than for bedrock recovery, it is still of small magnitude. In the (b) sub-figs., the recovered variable closely aligns with the true values. It is visible that areas or largest error are at the top and tail ends of the glacier.
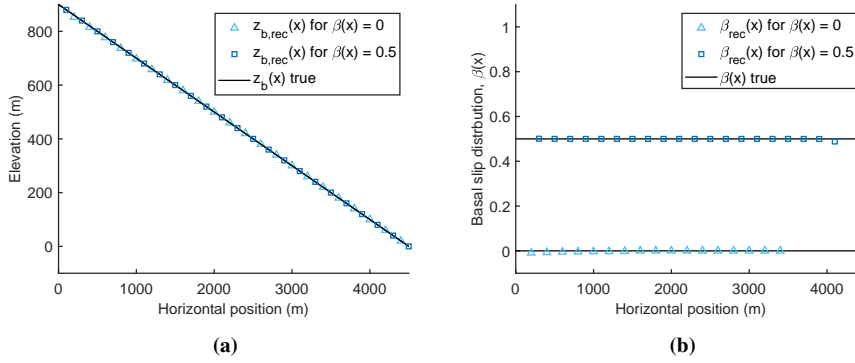

Fig. 7: Recovered bedrock (a) for non-constant basal slip where $z_b = f$ and corresponding recovered basal slip (b).
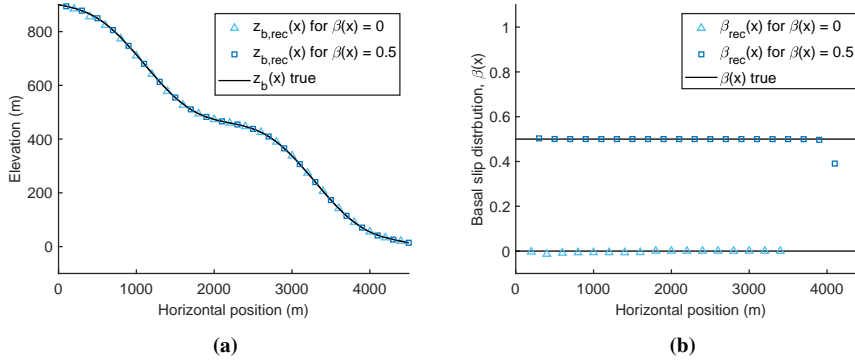

Fig. 8: Recovered bedrock (a) for constant basal slip where $z_b = f$ and corresponding recovered basal slip (b).
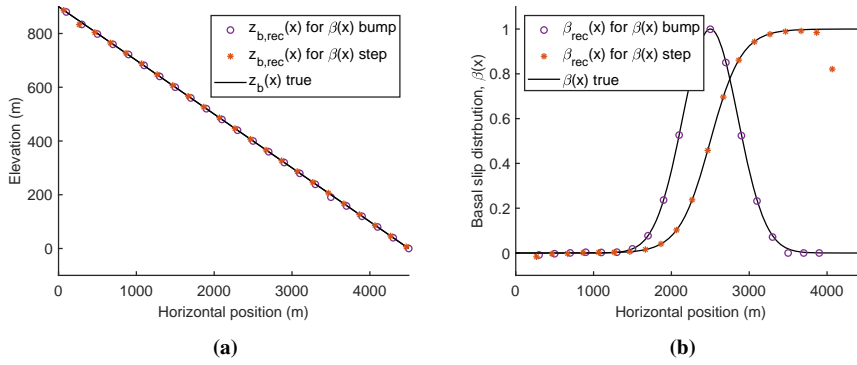
Fig. 9: Recovered bedrock (a) for non-constant basal slip where $z_b = f$ and corresponding recovered basal slip (b).
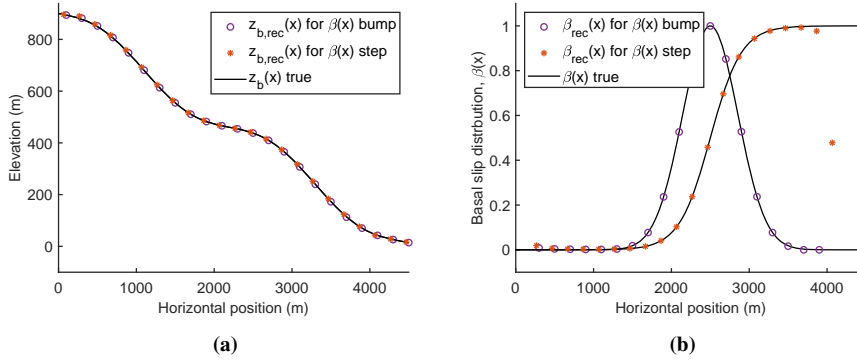

Fig. 10: Recovered bedrock (a) for non-constant basal slip where $z_b = b$ and corresponding recovered basal slip (b).

6 Sensitivity analysis

Glacier surface data in reality always has some noise. Therefore, for practical applications the method should be capable of handling noisy data. To evaluate the effect of noise on the inversion method, noise is added to each of the measured variables; S, u_s. Noise is added to synthetic surface data in the following way:

$$S_{noise} = S_{true} + \varepsilon n \max(H_{true}) \text{ and,} \tag{33}$$

$$u_{s,noise} = u_{s,true} + \varepsilon n (\max(u_{s,true} - \min u_{s,true}), \tag{34}$$

where $n \in [-1, 1]$ is randomly distributed. The amount of noise to be easily adjusted by choosing $\varepsilon \in [0, 1]$ where the larger the choice, the more noise. Once noise is added to surface data, the result is smoothed with a local regression using weighted linear least squares and a second degree polynomial model which assigns less weight to outliers in the regression. The local span for the regression is 20 % of the data points. Data outside six mean

Table 3: Associated errors for recovered bedrock profile elevation and basal slip distribution as defined by Eqs. (31) and (32).

Case		Relative errors	
$\beta(x)$	z_b	$E(z_{b,rec}, z_b)$	$E(\beta_{rec}, \beta)$
0	f	0.0057	0.2371
0	b	0.0085	0.3583
0.5	f	0.0003	0.0377
0.5	b	0.0006	0.0547
bump	f	0.0043	0.0109
bump	b	0.0025	0.0059
step	f	0.0036	0.1090
step	b	0.0054	0.1348

absolute deviations is given zero weight. Smoothing the data is important as $\frac{\partial S}{\partial x}$ appears regularly in the equations and needs be well defined. Examples of noise added to surface data as well as their smoothed counterparts can be found in the supplementary material.

This process is applied to all benchmark cases with both $\varepsilon = 0.1$ and $\varepsilon = 0.2$. An example of the results for 100 samples of noisy surface data using constant slip and a bumpy bedrock with $\varepsilon = 0.2$ are shown in Fig. 11. The solution envelope remains within 20% of the true value, indicating noise does not make the inversion method unstable. The envelope for the recovered basal slip distributions is much larger. Away from the glacier margins, the inversion remains within 20% of the true value. Near the ends, the noisy solution becomes unstable. This is not unexpected and reasons for solution error near the margins are discussed in the next section.
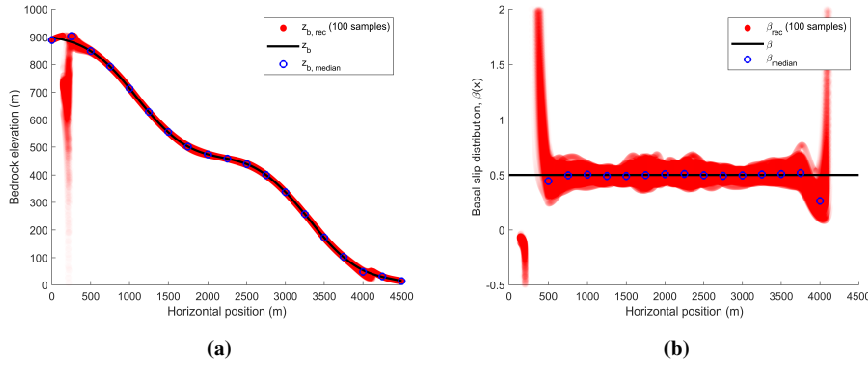
Fig. 11: Recovered bedrock elevation profile (a) and basal slip distribution (b) for 100 samples of noisy surface data where underlying bedrock is $z_b = b$ and $\beta = 0.5$. The solution envelope is given in red, the median solution as blue circles and the true as a black line for for reference. In this case, $\varepsilon = 0.2$.

7 Discussion

For each combination of bedrock elevation profile and basal slip distribution, the recovery of each input variable was good. Errors in the reconstructed bedrock elevation for all scenarios was negligibly small. Similarly for the basal slip distribution, though there were some relatively larger errors in this recovery. The largest errors in all cases arose at either the top or bottom end of the glacier.

At the top end of the glacier, there is a dome where the gradient of the free surface elevation is 0, in other words $\frac{\partial S}{\partial x} = 0$. Clearly, given Eq. (11) for surface velocity, this results in a stagnation point in the free surface. Due to this, no information about $\beta(x)$ or $H(x)$ can be recovered from Eq. (11). In Newton's method, this stagnation point presents as $F'(H) = 0$, which cannot be solved. Additionally, when $F'(H)$ becomes very small Newton's method becomes unstable due to division by $F'(H)$. To combat this, when $|\frac{\partial S}{\partial x}| \approx 0$, the previous solution for H is taken and the method skips to the next horizontal point.

At the bottom end of the glacier, $|\frac{\partial S}{\partial x}| \to \infty$. Because a finite number of points is used to approximate the derivative in places where it changes rapidly, such as at the bottom end, the approximation is worse. These approximation errors transfer across to the inverse solution. In addition, at the very top and very bottom where the ice ends, $\frac{\partial S}{\partial x}$ is discontinuous. This discontinuity gives rise to error also.

8 Conclusion

The results show that it is possible to accurately recover both the bedrock elevation profile and basal slip distribution of a glacier for given surface elevation and velocity in certain realistic synthetic cases. The method, although simple, is robust regardless of the underlying bedrock profile and basal slip distribution. This is a key result when considering the applicability of the method to 'real world' problems in which bedrock and basal slip are unlikely to be uniform. A logical next step in developing the method is testing performance in a three-dimensional flow.

Previous authors have focused on bedrock recovery in no-slip cases. That simplification gives rise to many interesting methods but neglects basal slip which plays a vital role in glacial evolution. Indeed, since basal slip can drastically change the height of the glacier due to dynamic thinning, the bedrock elevation recovery can have large error if this is not considered. The method presented here still returns the correct bedrock elevation profile and basal slip distribution with the more general inclusion of basal slip for certain broadly realistic synthetic cases. Further, a previously unknown implication is that a unique combination of bedrock elevation profile and basal slip distribution gives rise to unique surface elevation and velocity. Further studies into the generalised case are required to prove this.

References

1. Adhikari, S., J. Marshall, S.: Parameterization of lateral drag in flowline models of glacier dynamics. Journal of Glaciology **58**(212), 1119–1132 (2012). DOI DOI: 10.3189/2012JoG12J018. URL https://www.cambridge.org/core/article/parameterization-of-lateral-drag-in-flowline-models-of-glacier-dynamics/9C5836F192CE16F10F08DE750B1BFCAE
2. Adhikari, S., Marshall, S.J.: Improvements to shear-deformational models of glacier dynamics through a longitudinal stress factor. Journal of Glaciology **57**(206) (2011). URL http://www.csc.fi/english/pages/elmer
3. Alley, R.B., Blankenship, D.D., Bentley, C.R., Rooney, S.T.: Deformation of till beneath ice stream B, West Antarctica. Nature **322**(6074), 57–59 (1986). DOI 10.1038/322057a0. URL http://www.nature.com/articles/322057a0
4. {\O}strem, G.: Erts Data in Glaciology—An Effort to Monitor Glacier Mass Balance from Satellite Imagery. Journal of Glaciology **15**(73), 403–415 (1975). DOI 10.3189/S0022143000034511. URL https://www.cambridge.org/core/product/identifier/S0022143000034511/type/journal_article
5. Barcilon, V., MacAyeal, D.R.: Steady flow of a viscous ice stream across a no-slip/free-slip transition at the bed. Journal of Glaciology **39**(131), 167–185 (1993). DOI 10.3189/S0022143000015811. URL https://www.cambridge.org/core/product/identifier/S0022143000015811/type/journal_article
6. Bevan, S.L., Luckman, A., Khan, S.A., Murray, T.: Seasonal dynamic thinning at Helheim Glacier. Earth and Planetary Science Letters **415**, 47–53 (2015). DOI 10.1016/J.EPSL.2015.01.031. URL https://www.sciencedirect.com/science/article/pii/S0012821X15000588
7. Bierman, P.R., Montgomery, D.R.: Key Concepts in Geomorphology. W.H.Freeman & Co Ltd (2014)
8. Blatter, H., Greve, R., Abe-Ouchi, A.: Present State and Prospects of Ice Sheet and Glacier Modelling. Surveys in Geophysics **32**(4-5), 555–583 (2011). DOI 10.1007/s10712-011-9128-0. URL http://link.springer.com/10.1007/s10712-011-9128-0
9. Budd, W.F., Keage, P.L., Blundy, N.A.: Empirical Studies of Ice Sliding. Journal of Glaciology **23**(89), 157–170 (1979). DOI 10.3189/S0022143000029804. URL https://www.cambridge.org/core/product/identifier/S0022143000029804/type/journal_article
10. Cazenave, A., Gregory, J.M., Jevrejeva, S., Levermann, A., Merrifield, M.A., Milne, G.A., Nerem, R.S., Nunn, P.D., Payne, A.J., Pfeffer, W.T., Stammer, D., Unnikrishnan, A.S.: Sea level change. In: T. Stocker, D. Qin, G.K. Plattner, M. Tignor, S. Allen, J. Boschung, A. Nauels, Y. Xia, V. Bex, P. Midgley (eds.) Climate Change 2013: The Physical Science Basis. Contribution of Working Group I to the Fifth Assessment Report of the Intergovernmental Panel on Climate Change, chap. 13, pp. 1137–1216. Cambridge University Press, Cambridge, United Kingdom and New York, NY, USA. (2013)
11. Christoffersen, P., Tulaczyk, S.: Response of subglacial sediments to basal freeze-on 1. Theory and comparison to observations from beneath the West Antarctic Ice Sheet. Journal of Geophysical Research: Solid Earth **108**(B4) (2003). DOI 10.1029/2002JB001935. URL http://doi.wiley.com/10.1029/2002JB001935
12. Church, J.A., Clark, P.U., Cazenave, A., Gregory, J.M., Jevrejeva, S., Levermann, A., Merrifield, M.A., Milne, G.A., Nerem, S., Nunn, P.D., Payne, A.J., Pfeffer, W.T., Stammer, D., Unnikrishnan, A.S.: Sea Level Change. In: T.F. Stocker, G. Qin, K. Plattner, M. Tignor, S. Allen, J. Boschung, A. Nauels, Y. Xia, V. Bex, P.M. Midgley (eds.) Climate Change 2013: The Physical Science Basis. Contribution of Working Group I to the Fifth Assessment Report of the Intergovernmental Panel on Climate Change, chap. 13, pp. 1137 – 1216. Cambridge University Press, Cambridge, United Kingdom and New York, NY, USA. (2013)
13. Crüger, T., Fischer, H., von Storch, H.: What do accumulation records of single ice cores in Greenland represent? Journal of Geophysical Research: Atmospheres **109**(D21), n/a–n/a (2004). DOI 10.1029/2004JD005014. URL http://doi.wiley.com/10.1029/2004JD005014
14. Cuffey, K.M., Paterson, W.S.B.: The Physics of Glaciers. Elsevier Science & Technology Books (2010)
15. Environmeantal Protection Agency: Collecting Snow and Ice Data (2017). URL https://www.epa.gov/climate-indicators/collecting-snow-and-ice-data
16. Farinotti, D., Brinkerhoff, D.J., Clarke, G.K.C., Fürst, J.J., Frey, H., Gantayat, P., Gillet-Chaulet, F., Girard, C., Huss, M., Leclercq, P.W., Linsbauer, A., Machguth, H., Martin, C., Maussion, F., Morlighem, M., Mosbeux, C., Pandit, A., Portmann, A., Rabatel, A., Ramsankaran, R., Reerink, T.J., Sanchez, O., Stentoft, P.A., Singh Kumari, S., van Pelt, W.J.J., Anderson, B., Benham, T., Binder, D., Dowdeswell, J.A., Fischer, A., Helfricht, K., Kutuzov, S., Lavrentiev, I., McNabb, R., Gudmundsson, G.H., Li, H., Andreassen, L.M.: How accurate are estimates of glacier ice thickness? Results from ITMIX, the Ice Thickness Models Intercomparison eXperiment. The Cryosphere **11**(2), 949–970 (2017). DOI 10.5194/tc-11-949-2017. URL https://www.the-cryosphere.net/11/949/2017/

17. Flament, T., Rémy, F.: Dynamic thinning of Antarctic glaciers from along-track repeat radar altimetry. Journal of Glaciology **58**(211), 830–840 (2012). DOI 10.3189/2012JoG11J118. URL https://www.cambridge.org/core/product/identifier/S0022143000208885/type/journal_article

18. Fowler, A.C.: Sliding with Cavity Formation. Journal of Glaciology **33**(115), 255–267 (1987). DOI 10.3189/S0022143000008820. URL https://www.cambridge.org/core/product/identifier/S0022143000008820/type/journal_article

19. Gessese, A., Heining, C., Sellier, M., Mc Nish, R., Rack, W.: Direct reconstruction of glacier bedrock from known free surface data using the one-dimensional shallow ice approximation. Geomorphology **228**, 356–371 (2015). DOI 10.1016/J.GEOMORPH.2014.09.015. URL https://www.sciencedirect.com/science/article/pii/S0169555X14004905

20. Glen, J.W.: Experiments on the Deformation of Ice. Journal of Glaciology **2**(12), 111–114 (1952). DOI 10.3189/S0022143000034067. URL https://www.cambridge.org/core/product/identifier/S0022143000034067/type/journal_article

21. Greve, R., Blatter, H.: Dynamics of Ice Sheets and Glaciers. Advances in Geophysical and Environmental Mechanics and Mathematics. Springer Berlin Heidelberg, Berlin, Heidelberg (2009). DOI 10.1007/978-3-642-03415-2. URL http://link.springer.com/10.1007/978-3-642-03415-2

22. Heining, C., Sellier, M.: Direct Reconstruction of Three-dimensional Glacier Bedrock and Surface Elevation from Free Surface Velocity. AIMS Geosciences **2**(1), 45–63 (2016). DOI 10.3934/geosciences.2016.1.63. URL http://www.aimspress.com/journal/geosciences

23. Hubbard, B., Glasser, N.: Field Techniques in Glaciology and Glacial Geomorphology (2005)

24. Hutter, K.: The Effect of Longitudinal Strain on the Shear Stress of an Ice Sheet: In Defence of Using Stretched Coordinates. Journal of Glaciology **27**(95), 39–56 (1981). DOI 10.3189/S0022143000011217. URL https://www.cambridge.org/core/product/identifier/S0022143000011217/type/journal_article

25. Iverson, N.R., Hanson, B., Hooke, R.L., Jansson, P.: Flow mechanism of glaciers on soft beds. Science (New York, N.Y.) **267**(5194), 80–1 (1995). DOI 10.1126/science.267.5194.80. URL http://www.ncbi.nlm.nih.gov/pubmed/17840062

26. Jiskoot, H.: Dynamics of Glaciers. In: V.P. Singh, P. Singh, U.K. Haritashya (eds.) Encyclopedia of Snow, Ice and Glaciers, pp. 245–256. Springer Netherlands, Dordrecht (2011). DOI 10.1007/978-90-481-2642-2_127. URL https://doi.org/10.1007/978-90-481-2642-2_127

27. Kaser, G., Fountain, A., Jansson, P.: A manual for monitoring the mass balance of mountain glaciers. Unesco (2003). URL https://globalcryospherewatch.org/bestpractices/docs/UNESCO_manual_glaciers_2003.pdf

28. Kleman, J., Glasser, N.F.: The subglacial thermal organisation (STO) of ice sheets. Quaternary Science Reviews **26**(5-6), 585–597 (2007). DOI 10.1016/J.QUASCIREV.2006.12.010. URL https://www.sciencedirect.com/science/article/pii/S0277379106003490

29. Lal, D., Nishiizumi, K., Arnold, J.R.: In situ cosmogenic 3 H, 14 C, and 10 Be for determining the net accumulation and ablation rates of ice sheets. Journal of Geophysical Research **92**(B6), 4947 (1987). DOI 10.1029/JB092iB06p04947. URL http://doi.wiley.com/10.1029/JB092iB06p04947

30. Le Meur, E., Gagliardini, O., Zwinger, T., Ruokolainen, J.: Glacier flow modelling: a comparison of the Shallow Ice Approximation and the full-Stokes solution. Comptes Rendus Physique **5**(7), 709–722 (2004). DOI 10.1016/J.CRHY.2004.10.001. URL https://www.sciencedirect.com/science/article/pii/S1631070504001732

31. Lliboutry, L.: General Theory of Subglacial Cavitation and Sliding of Temperate Glaciers. Journal of Glaciology **7**(49), 21–58 (1968). DOI 10.3189/S0022143000020396. URL https://www.cambridge.org/core/product/identifier/S0022143000020396/type/journal_article

32. Martin, N., Monnier, J.: Inverse rheometry and basal properties inference for pseudoplastic geophysical flows. European Journal of Mechanics - B/Fluids **50**, 110–126 (2015). DOI 10.1016/j.euromechflu.2014.11.011. URL https://linkinghub.elsevier.com/retrieve/pii/S0997754614001733

33. Monnier, J., des Boscs, P.E.E.: Inference of the Bottom Properties in Shallow Ice Approximation Models. Inverse Problems **33**(11) (2017). DOI 10.1088/1361-6420/aa7b92. URL https://doi.org/10.1088/1361-6420/aa7b92

34. Nye, J.: The flow law of ice from measurements in glacier tunnels, laboratory experiments and the Jungfraufirn borehole experiment. Proceedings of the Royal Society of London. Series A. Mathematical and Physical Sciences **219**(1139), 477–489 (1953). DOI 10.1098/rspa.1953.0161. URL http://www.royalsocietypublishing.org/doi/10.1098/rspa.1953.0161

35. Pritchard, H.D., Arthern, R.J., Vaughan, D.G., Edwards, L.A.: Extensive dynamic thinning on the margins of the Greenland and Antarctic ice sheets. Nature **461**(7266), 971–975 (2009). DOI 10.1038/nature08471. URL http://www.nature.com/articles/nature08471

36. Rowan, A.V., Quincey, D.J., Gibson, M.J., Glasser, N.F., Westoby, M.J., Irvine-Fynn, T.D., Porter, P.R., Hambrey, M.J.: The sustainability of water resources in High Mountain Asia in the context of recent and future glacier change. Geological Society Special Publication **462**(1), 189–204 (2018). DOI 10.1144/SP462.12

37. Schwikowski, M., Schläppi, M., Santibañez, P., Rivera, A., Casassa, G.: Net accumulation rates derived from ice core stable isotope records of Pío XI glacier, Southern Patagonia Icefield. The Cryosphere **7**, 1635–1644 (2013). DOI 10.5194/tc-7-1635-2013. URL www.the-cryosphere.net/7/1635/2013/

38. Shuman, C.A., Berthier, E., Scambos, T.A.: 2001–2009 elevation and mass losses in the Larsen A and B embayments, Antarctic Peninsula. Journal of Glaciology **57**(204), 737–754 (2011). DOI 10.3189/002214311797409811. URL https://www.cambridge.org/core/product/identifier/S002214300020422X/type/journal_article

39. Weertman, J.: On the Sliding of Glaciers. Journal of Glaciology **3**(21), 33–38 (1957). DOI 10.3189/S0022143000024709. URL https://www.cambridge.org/core/product/identifier/S0022143000024709/type/journal_article

40. Wilchinsky, A., Chugunov, V.: Modelling ice flow in various Glacier zones. Journal of Applied Mathematics and Mechanics **65**(3), 479–493 (2001). DOI 10.1016/S0021-8928(01)00054-5. URL https://www.sciencedirect.com/science/article/pii/S0021892801000545